Bioimaging **6** (1998) 177–185. Printed in the UK PII: S0966-9051(98)99112-2

# Multifocal multiphoton microscopy: a fast and efficient tool for 3-D fluorescence imaging

**Martin Straub and Stefan W Hell**

High Resolution Optical Microscopy Group, Max-Planck-Institute for Biophysical Chemistry, D-37070 Göttingen, Germany

Submitted 21 October 1998, accepted 6 November 1998

**Abstract.** Multifocal multiphoton microscopy (MMM) is an efficient and technically simple method for generating multiphoton fluorescence images. Featuring the high axial resolution of confocal and multiphoton scanning microscopes, MMM also achieves high speed in 3-D microscopy. In this paper, examples of fast-mode 3-D microscopy are given including imaging of fixed brain tissue as well as living PC12 cells. The imaging speed of MMM is solely determined by the fluorescence photon flux, so that in practice, for brightly fluorescent specimens, a whole stack of about 50 images of 30–70 $\mu$m diameter can be acquired within a few seconds. MMM represents a significant advance towards high speed nonlinear optical tomography of fluorescent specimens.

**Keywords:** fluorescence microscopy, two-photon, multifocal, three-dimensional, optical cell tomography, PC12 cells, dendritic spines

M This article features multimedia enhancements available from the abstract page in the online journal; see `http://www.iop.org`.

## 1. Introduction

Over the past few decades several techniques have been established for biological microscopy. In the 1980s confocal scanning microscopy emerged as a powerful method for three-dimensional (3-D) imaging of biological specimens [1]. More recently, multiphoton excitation microscopy [2–8] has proved to be a useful complement to the single-photon excitation confocal predecessor. In multiphoton fluorescence microscopy the simultaneous absorption of two or three near-infrared (NIR) photons yields a 3-D resolution very close to that of a standard confocal microscope. As simultaneous multiphoton absorption predominantly occurs in the focal region, photobleaching and photodamage are confined to the focal plane. Multiphoton fluorescence microscopy excels due to its inherent sectioning capability, deeper penetration into scattering specimens and by the fact that NIR light is more benign to living cells.

Two-photon microscopy is usually carried out with expensive pulsed lasers, such as the mode-locked titanium:sapphire (Ti:Sa) laser providing pico- or sub-picosecond pulses at $\sim$ 80 MHz repetition rate [6, 9]. Due to its tunability from 700 nm to 1050 nm, the Ti:Sa laser is arguably the most suitable light source for multiphoton microscopy [2]. In its standard configuration the Ti:Sa emits 500–1000 mW of time-averaged power and, in the case of a large frame pump laser, the emission can reach 2000 mW. Focused down by a high aperture lens to a $\sim$ 300 nm diameter focal spot, the beam of such a laser can produce focal irradiances of the order of 100 TW/cm$^2$. Although this value is achieved only for a few hundred femtoseconds, it is much higher than most materials can withstand [10]. In practice the maximum tolerable intensity in biological systems as well as fluorophores is about 100 times lower. Consequently, with a high numerical aperture (NA) lens such as NA 1.2 and higher, a maximum of 5–20 mW can be focused to the same point in the sample [11]. As a result, only about 5% or less of the pulsed Ti:Sa laser light is used for imaging; the rest is dumped.

Maximum power is largely determined by nonlinear optical effects and, therefore, to a much greater extent by the peak power than the time-averaged value. This has become evident in two-photon microscopy using comparatively long pulses of 7 ps, which inevitably involve lower peak intensities and higher average power [12]. Even continuous-wave two-photon excitation microscopy of live cell nuclei has been demonstrated at an average excitation

  

power of 200 mW [13]. It follows that a much larger fraction of the Ti:Sa laser light is usable in the imaging if the light is evenly distributed among many foci at the sample. Moreover, the simultaneous use of parallel beams substantially increases the image acquisition speed in multiphoton microscopy. Making use of all of the laser light and reducing the acquisition time was the main rationale in the development of multifocal multiphoton microscopy by us [14–16] and also by others [17].

In MMM, the near-infrared beam of a Ti:Sapphire laser impinges on an array of microlenses that separate the beam into a number of beamlets. The beamlets are focused simultaneously onto the sample. Each beamlet carries enough light in order to ensure sufficient but non-damaging multiphoton excitation. The quadratic or cubic dependence of the fluorescence signal on the excitation intensity has the effect that the fluorescence stems only from the focal region of each beamlet. The multiple signals are imaged onto a CCD camera in much the same way as in a conventional microscope. The microlenses are arranged in a helical order so that fast rotation of the disk ensures complete and fast coverage of the focal plane. Such a configuration does not require synchronization and provides inherently 3-D imaging. The only compromise with respect to standard multiphoton microscopy arises with very strongly scattering samples, in which the imaging of the fluorescence light onto the CCD camera leads to a finite cross-talk between the pixels. We emphasise that the foci *as such* do not cross-talk in a properly designed multifocal multiphoton microscope. Therefore, in contrast to real-time two-photon imaging using line-scanning [18], resolution is not traded off against speed.

It is important for routine applications that the quick rotation of the disk allows direct visual viewing of two-photon excitation generated images. In addition, MMM is a highly flexible method that can be readily combined with other camera based imaging techniques. Recently, 3-D fluorescence lifetime imaging with picosecond precision and 200 ps resolution was demonstrated by combining MMM with gated, intensified camera recording [16]. This system opens up the prospect of developing a very efficient way of performing 4D microscopy.

In this paper, after a brief description of the experiment, examples of biological imaging are given along with a description of the recording conditions. We show that 3-D image stacks of fluorescent specimens can be gained within a comparatively short period of time of only a few seconds or even less.

## 2. Experimental procedure

The multifocal multiphoton microscope sketched in figure 1(*a*) features a modelocked Ti:sapphire laser, beam expansion optics ($L_1$, $L_2$), the microlens array disk, and intermediate relay optics ($L_4$, $L_5$), attached to an inverted conventional microscope (a Leica DM-IRB). In the wavelength range between 760 nm and 920 nm the average power of our Ti:Sa laser (Mira 900F, Coherent, Palo Alto) was 1.6–2.0 W. The outer region of the expanded beam was cut off by a stop, so as to achieve a more uniform illumination. Redundant Argon ion pump laser light was removed by an OG 550-edge filter (Schott, Mainz). The laser beam impinged on the rotating microlens disk whose basic features have been recently described [15]. The beam was divided into 15–25 beamlets which were focused into a virtual prefocusing plane (PFP) located 4.5 mm behind the disk. In contrast to initial studies, the intermediate space between the microlenses was largely obstructed by a metal foil, thus preventing unfocused light from entering the microscope. This simple measure reduces a small but otherwise noticeable fluorescence background in thick specimens.

Changing intermediate optics ($L_3$, $L_4$) allowed us to vary the number and the distance of foci in the focal plane. The intermediate optical arrangement also ensured that each beamlet overilluminated the back-aperture of the objective lens, so as to render an uncompromised intensity point-spread-function at each focus. Inside the microscope fluorescence was separated from the infrared laser light by a dichroic mirror and imaged onto a CCD-camera (Imager 3L, La Vision, Göttingen). Remaining infrared light was absorbed by an appropriate filter combination consisting of 2–3 mm thick BG 39 blue-glass, or a combination of 1 mm KG3 glass (Schott, Mainz) and two custom-made interference filters. For wavelengths shorter than 750 nm, the latter transmitted about 80% of the fluorescence while suppressing more than five orders of magnitude at longer wavelengths.

Figure 1(*b*) shows an image of the fluorescence spots in a uniform sea of rhodamine 6G dissolved in immersion oil as generated by the foci of the resting microlens disk. Notice the slight tilt of the focal array due to the helical arrangement of the microlenses. Rotation of the disk yielded a dense coverage of the focal plane. Figure 1(*c*) was recorded at a disk rotation frequency of 75 Hz. Since the array features 5 independent sections, the scan rate amounted to $5 \times 75 = 375$ frames per second. Both images were taken at a laser wavelength of 765 nm using an oil immersion objective (Leica Plan APO 100×, NA 1.4) in combination with the 1.6× tube lens of the microscope. The exposure time was 50 ms. The average power in a single focus at the sample was 2.7 mW. For 160× magnification, the distances between the foci were $\sim 5.3\ \mu$m. The scan frame rate of 375 Hz would have allowed image acquisition times on the order of 3 ms, but for a 640 × 480 pixel image, the frame rate was confined to about 15 ms per image due to the limited read-out rate of the camera in use. However, given enough fluorescence light and a faster and more sensitive camera, frame rates of this order are feasible. In fact, the limitation is set only by

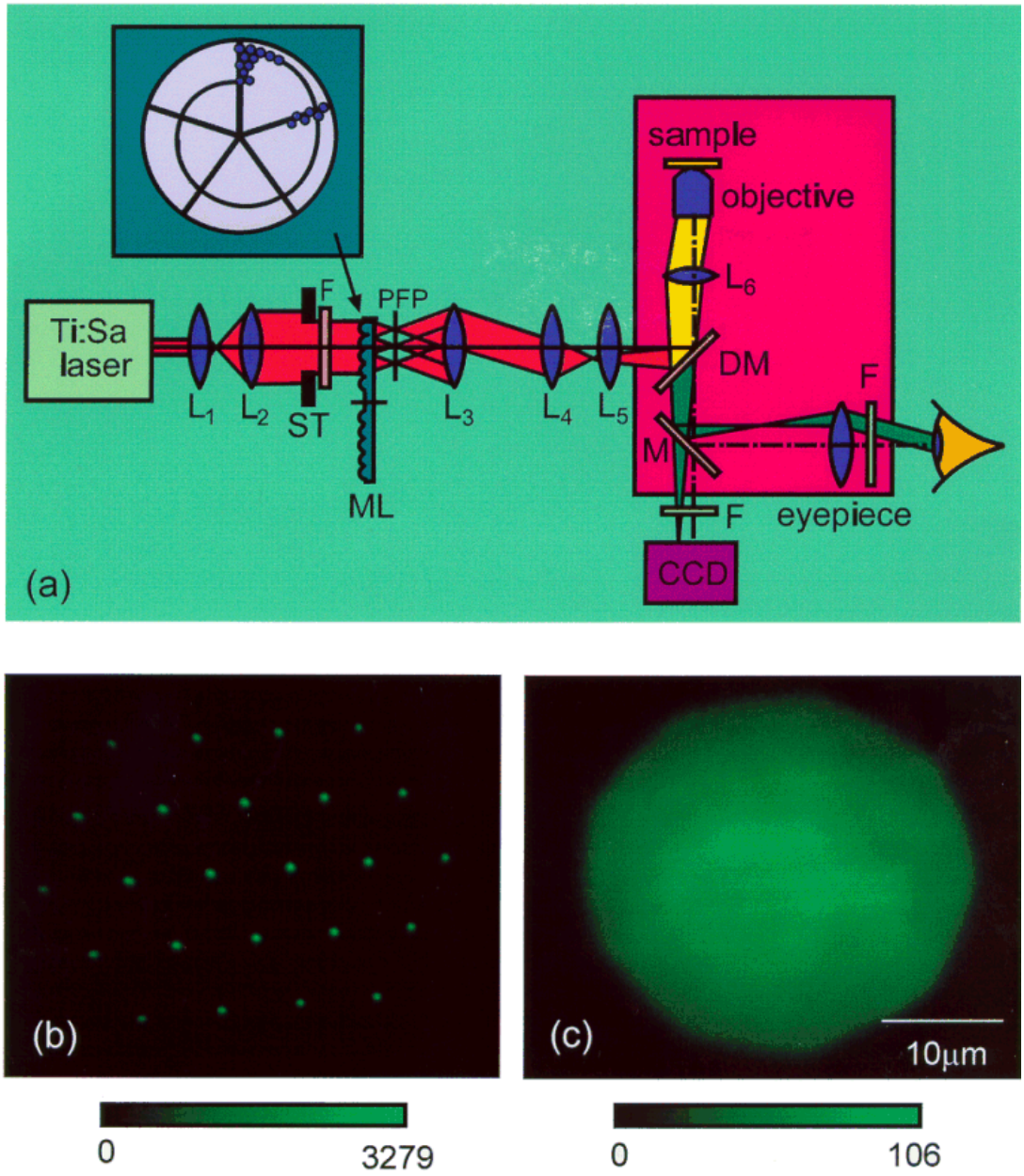


**Figure 1.** (*a*) Experimental set-up of the multifocal multiphoton microscope; (*b*) two-photon excitation foci produced in fluorescent solution by the resting and (*c*) rotating microlens disk. Ti:sapphire laser pulses are expanded by a telescope ($L_1$, $L_2$) before passing the microlens array. The intermediate optics ($L_3$–$L_5$) feed the beamlets into the microscope and project them onto the sample as an array of high resolution foci. Fluorescence light is transmitted by the dichroic mirror (DM) and is detected either by a CCD camera or by visual observation.

the fluorescence photon flux. Unlike galvanometer-based scanners, MMM does not involve scanning dead times.

Due to the elliptically shaped profile of the laser beam the illumination intensity dropped off to about 80% in the horizontal and 60% in the vertical direction. This effect was visible both for the standing and the rotating microlens disk. We chose intermediate optics such that for a 100× magnification objective the whole field of view was 30 $\mu$m in diameter. We note that while the lateral resolution of MMM is that of conventional fluorescence microscopy calculated at the fluorescence wavelength, the axial resolution is that of a single beam multiphoton excitation fluorescence microscope.

## 3. Results

For all experiments the important parameters such as wavelength, average power, stains, filters, objective lenses,

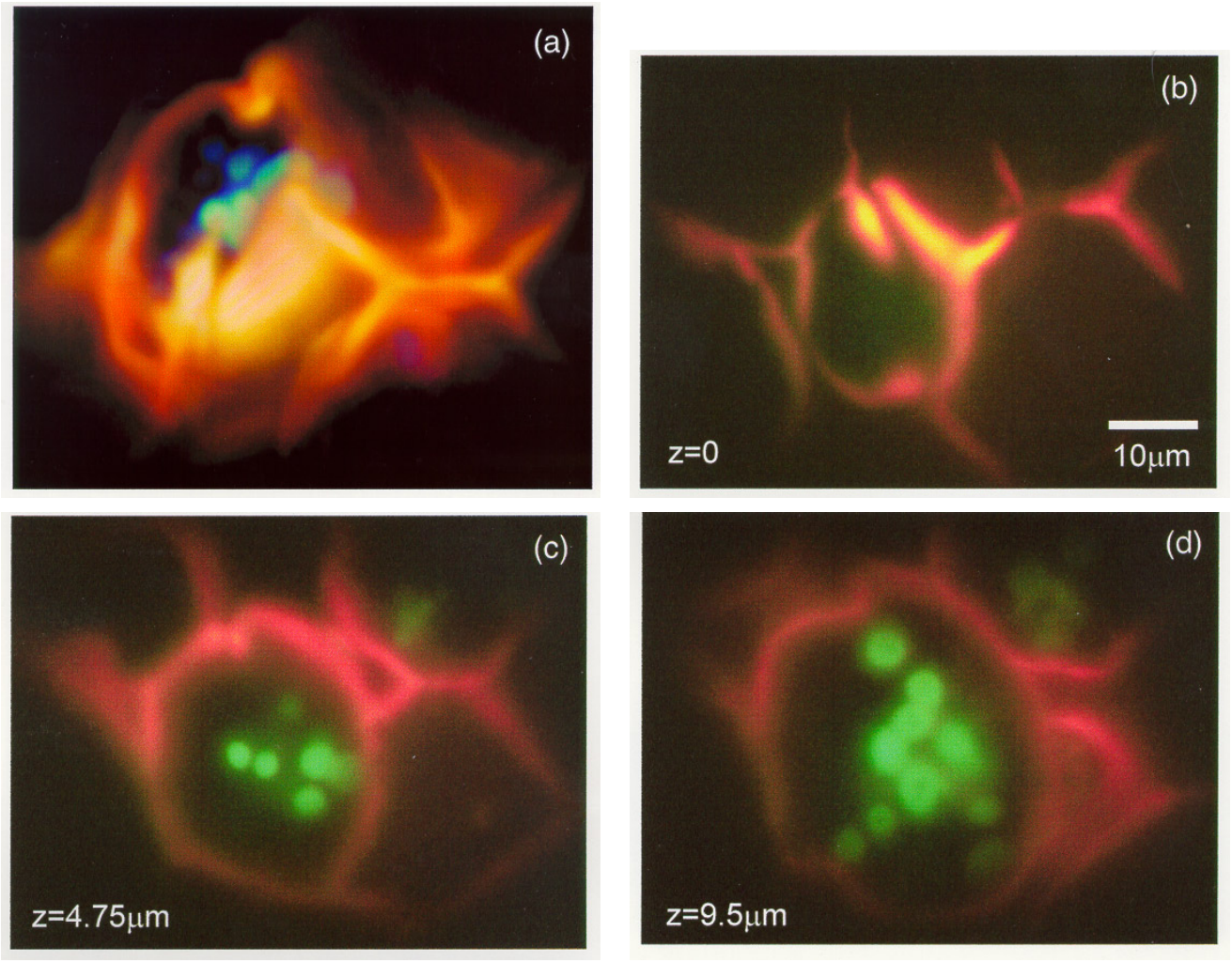


**Figure 2.** (*a*) Volume-rendered reconstruction from a stem of *Prionium* labelled with safranin-fast green; (*b–d*) shows three representative $XY$-slices. The data consist of of two different fluorescence channels: the cell walls (red) and the amyloplasts (green). The images were taken with a 100× oil immersion objective (NA 1.4) at an excitation wavelength of 895 nm.

M A *Quick-Time* movie of this figure is available from the article's abstract page in the online journal; see `http://www.iop.org`.

distance between slices, and exposure times are summarized in table A1 in appendix A. The 3-D images discussed here can be accessed as *Quick-Time* movies from the electronic version of this paper. The following figures constitute only excerpts of complete 3-D data stacks.

Figure 2 shows three representative $XY$-slices of an image stack taken from a stem of *Prionium* and labelled with safranin-fast green (*b–d*). Figure 2(*a*) shows the corresponding volume-rendered reconstruction. The cell walls fluoresced predominantly in the red regime, whereas the amyloplasts inside the cells emitted mainly in the green. The cell walls and the amyloplasts were consecutively recorded by employing different sets of filters in front of the camera (see table 1). In Figure 2 the two-colour images represent the corresponding two fluorescence channels. *Prionium* was recorded with the 100× oil immersion objective at 895 nm and by using a total average power of 1.8 W, of which after separation into ∼ 15 beamlets about 105 mW reached the focal plane. Each stack consisted of 41 $XY$-images that were 790 nm apart; each slice was acquired within 200 ms.

Figure 3 shows images of living PC12 cells of different size in physiological buffer attached to poly-D-lysine coated glass coverslips, vitally stained with acridine orange (Molecular Probes Inc., Eugene, OR, USA). A 3-D reconstruction of a data stack is displayed as viewed from different perspectives (*a*). Acridine orange bound to nuclear DNA emits in the green (525 nm), whereas dye accumulated within acidic organelles generates fluorescence in the red (650 nm). Like figure 2, figure 3(*a*) is also a two-fluorescence channel recording. Each channel was taken with a suitable combination of emission filters (see table 1). For the nuclei (green) a D520/60 interference

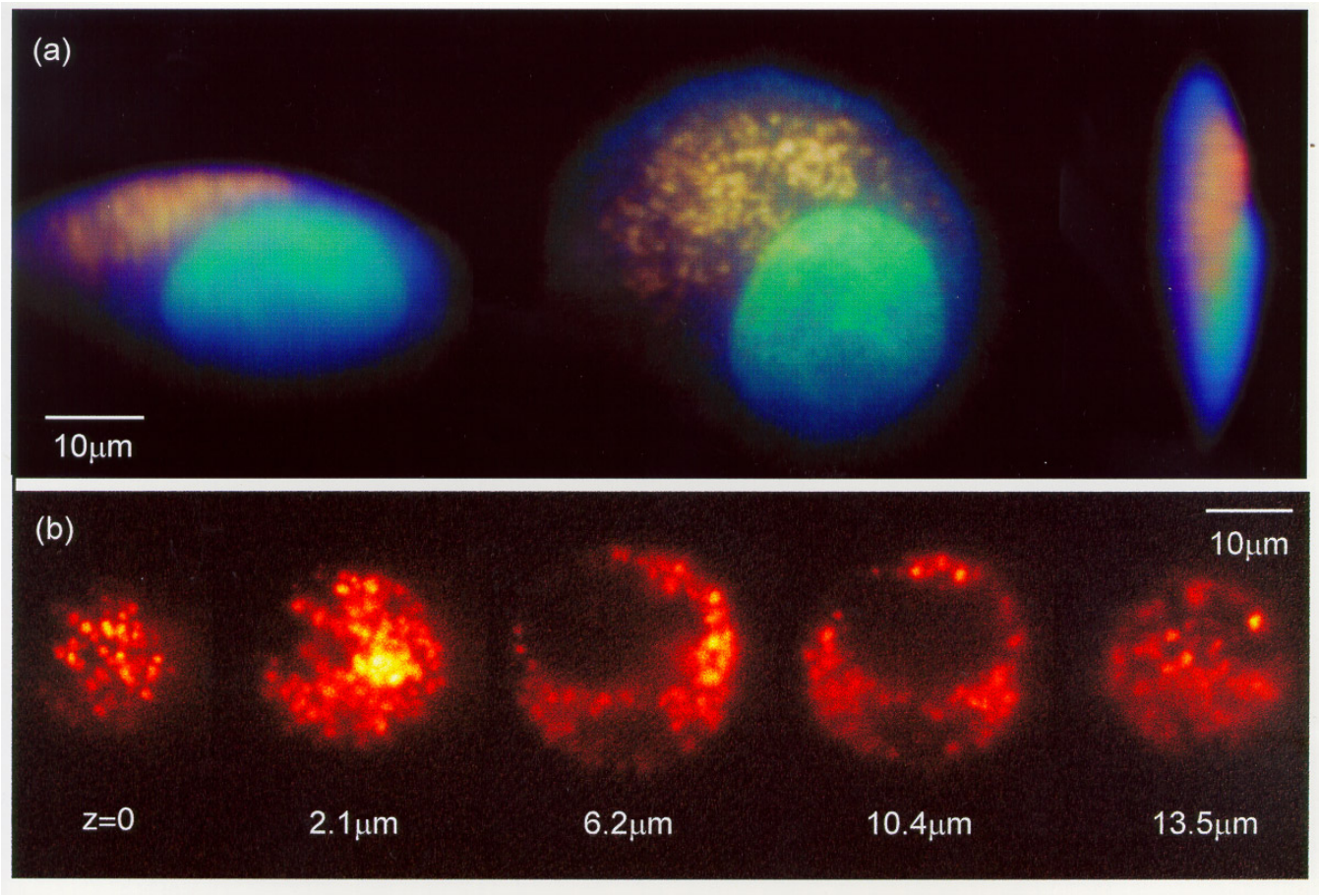


**Figure 3.** (*a*) Three perspectives of a volume-rendered 3-D reconstruction of a live PC12 cell stained with acridine orange. The cell is shown from the top (centre), tilted by about 60° along the horizontal axis (left) and rotated by 90° around the vertical axis (right). The DNA bound acridine orange in the nucleus emits at 525 nm (green) and dye accumulated within acidic organelles fluoresces at 650 nm (red). In (*b*) a sequence of slices through a typically shaped PC12 cell shows only the red component. While for the reconstruction in (*a*) each $XY$-slice was recorded within 200 ms, for the $XY$-slices in (*b*) only 75 ms exposure time were used. The images were recorded with a 60× water immersion objective combined with the 1.6× tube lens; the excitation wavelength was 895 nm.

M A *Quick-Time* movie of this figure is available from the article's abstract page in the online journal; see `http://www.iop.org`.

filter (Chroma, Brattleboro, VT, USA) was used, whereas the acidic organelles (red) were recorded by filtering the fluorescence with 3 mm of OG590 glass (Schott, Mainz). Figure 3(*b*) depicts 5 slices through another PC12 cell, of which only the red fluorescence was recorded. In the cell shown in (*b*) many acidic organelles are visible, with those close to the cell membrane probably representing pools of exocytotic vesicles. The data were taken as a stack of 31 $XY$-images recorded in axial steps of 1.04 $\mu$m. The objective lens was an Olympus water immersion lens (60×, NA 1.2) used together with a 1.6× tube lens. The laser operated at 895 nm; the used total laser average power was 105 mW at the sample and was distributed to $\sim$ 15 foci. The recording time was 200 ms and 75 ms for (*a*) and (*b*), respectively.

A straightforward change in the optical path allowed us to direct the fluorescence to the eyepiece. We protected our eyes from the intense laser radiation by placing 2.5 mm thick BG39 blue glass into the optical path of the eyepieces. The blue glass efficiently absorbed the NIR light as well as a fraction of the longer wavelengths of the red regime. The residual visible range (350–620 nm) was largely unattenuated so that the two-photon images of the stained live PC12 cells could be observed through the eyepiece in very nearly their true colours.

Figure 4 shows a dendritic branch of a Lucifer Yellow filled neuronal cell from the temporal cortex of a gerbil *(Meriones unguiculatus)*. Dye injections into neurons were performed in brain slices of $\sim$ 100 $\mu$m thickness previously fixed with formaldehyde. After Lucifer Yellow labelling the brain sections were immunocytochemically processed using an FITC-conjugated antibody against Lucifer Yellow and finally embedded in SlowFade (Molecular Probes). Along the dendritic process tiny protrusions of different size and shape are clearly visible. These so-called dendritic spines represent the postsynaptic part of a special type of synaptic

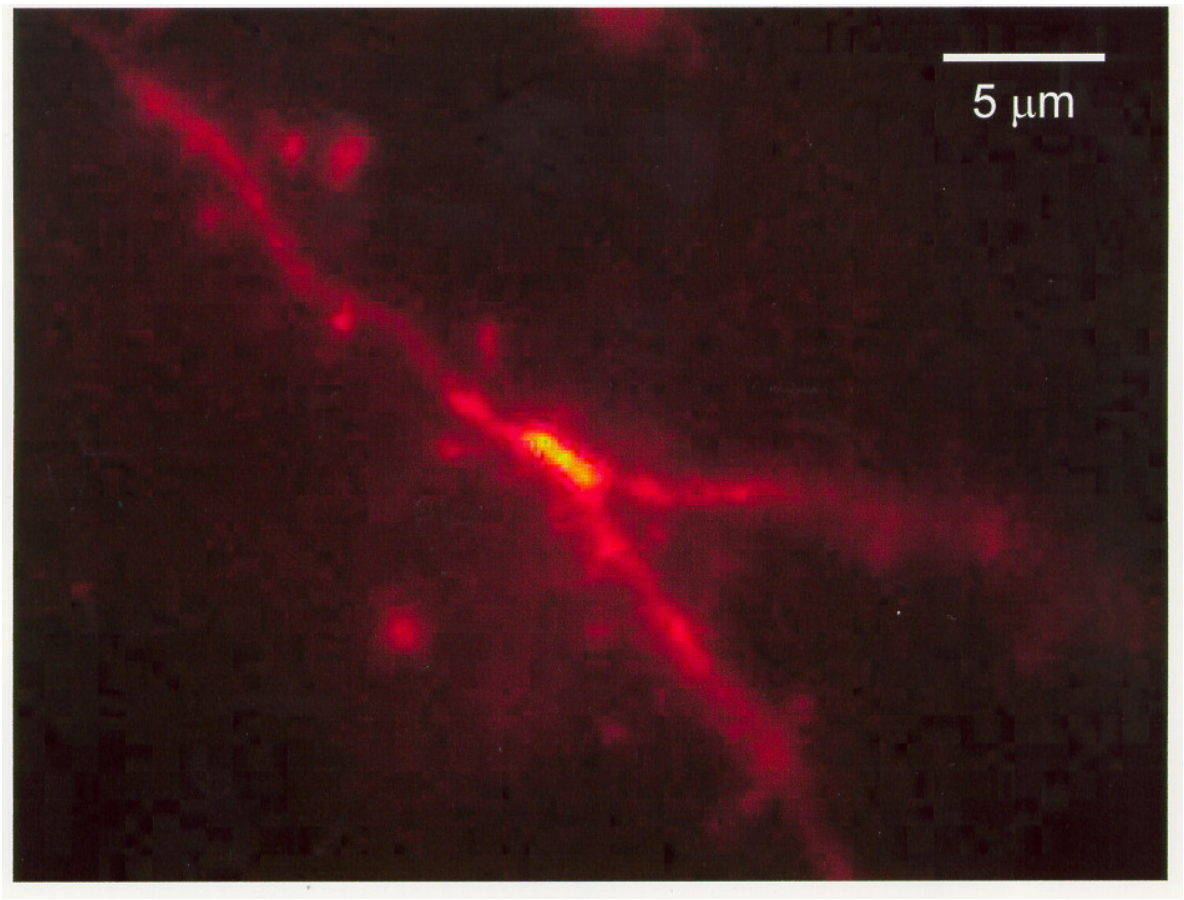


**Figure 4.** Optical section from an image stack through a dendritic process from a dye-labelled neuron in the temporal cortex of a gerbil *(Meriones unguiculatus)*. The neuron was iontophoretically injected with the fluorescent dye Lucifer Yellow after fixation of the brain tissue. Small spines of different shape protruding from the dendrite are clearly recognizable, although some haze blurs the vicinity of the dendritic process. The slight haze around the dendrite is probably due to scattering of fluorescent light by the surrounding brain tissue. The picture was taken with 96× magnification with a water immersion objective (60×, NA 1.2). The excitation wavelength was 780 nm.

M A *Quick-Time* movie of this figure is available from the article's abstract page in the online journal; see `http://www.iop.org`.

contacts and build the structural basis for interneuronal communication as well as a substrate for morphological changes during learning and memory processes [19, 20].

Although the image resolution was high enough to visualise the spines, which usually are of submicron dimensions, some haze is recognizable around the dendrites. This phenomenon can be explained by scattering of fluorescence light within the rather thick tissue slice. As the scattering length scale of visible light in brain tissue is in the order of 200 $\mu$m [10, 21, 22], an appreciable amount of the emitted fluorescence light is expected to be scattered in the immediate vicinity of the dendrites. The occurrence of haze in images of highly scattering samples is a drawback of multifocal multiphoton microscopy compared with single beam two-photon excitation microscopy with large area detection. In the latter case, serial data acquisition ensures that the fluorescence light always originates from the focal region, whereas in our camera-based system the imaging of strongly scattered fluorescence light onto the camera leads to a residual blur—at least at the present state of development. Nevertheless, the fact that we use NIR light should allow us to penetrate deeper into the specimen.

The image in figure 4 was taken within 1.0 s and was part of a 3-D data stack recorded with 410 nm axial distances between the $XY$-planes. The images were recorded with a water immersion objective (NA 1.2) at a total magnification (including the tube lens) of 96. The laser was operated at a wavelength of 780 nm, and the average power of about 110 mW at the sample was distributed among $\sim$ 20 foci. Fluorescence light was filtered with 2.5 mm of BG 39.

When increasing the intensity of the laser above $\sim$ 10–20 mW, one could visually observe the appearance of sudden bright luminescence spots in certain samples [23]. An advantage of MMM is the fact that optically limiting phenomena can be easily observed with the eye so that for a particular application safe power levels can be adjusted by visual observation. In figure 5 we show

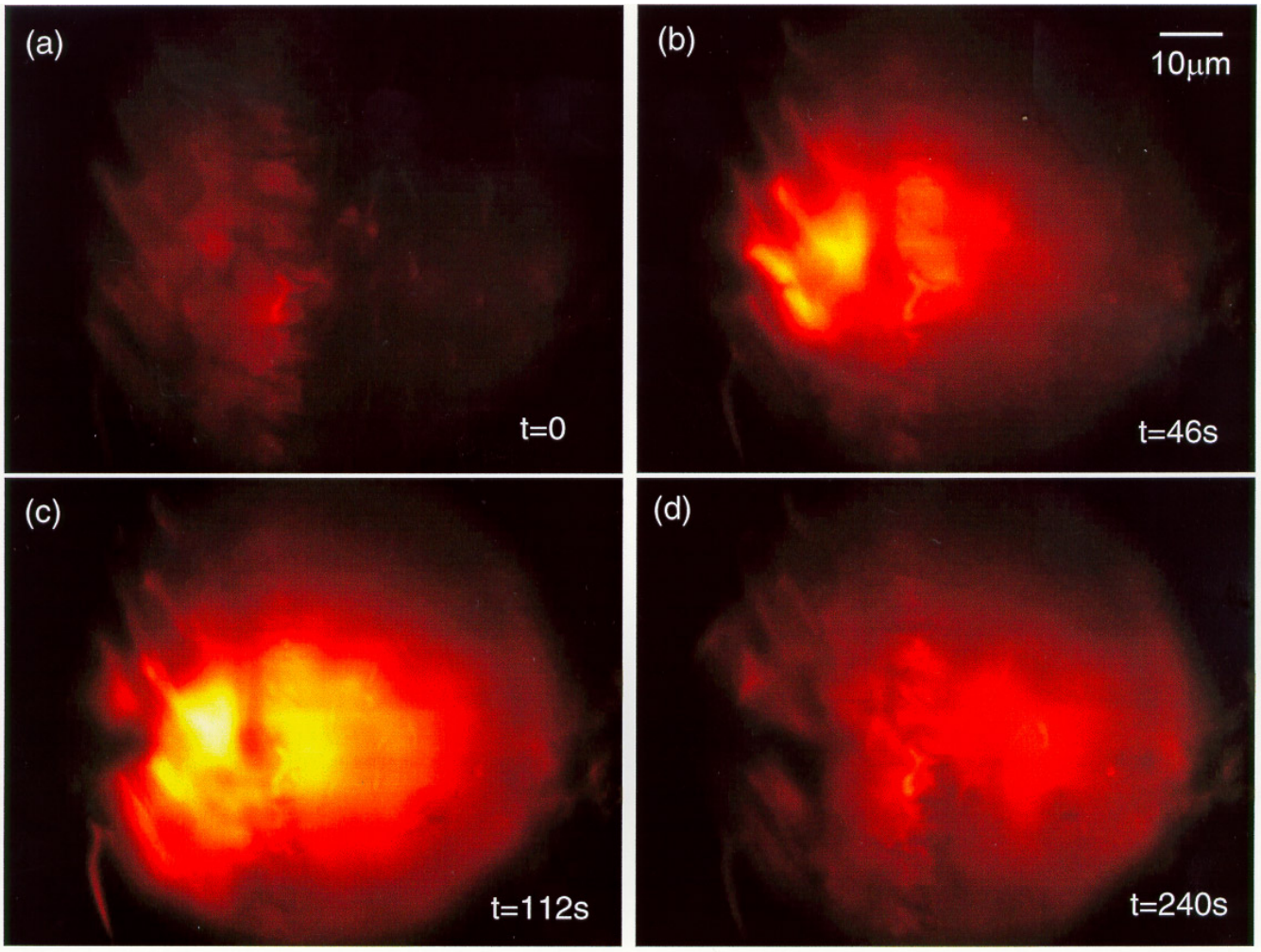


**Figure 5.** Autoluminescence of a wing of *Drosophila melanogaster* (*a*) for a laser power of 1.8 mW per focus, and (*b–d*) at different time points after increasing the power to 3.8 mW. At the higher laser power photochemical reactions were observed as sudden onsets of bright luminescence.

M A *Quick-Time* movie of this figure is available from the article's abstract page in the online journal; see `http://www.iop.org`.

four recordings of a time sequence of a slice through an unstained wing of *Drosophila melanogaster* embedded in a 6:1 mixture of phenol and lactic acid. The images were taken successively at 775 nm with an individual exposure time of 2.0 s. In figure 5(*a*) the power of a single beamlet amounted to $\sim$ 1.8 mW in the focus, and the total power in the focal plane of $\sim$ 40 mW was divided into $\sim$ 25 foci. Under these conditions luminescence emission was constant on a timescale of 10 s. However, when the power was raised to $\sim$ 3.8 mW per beamlet we could observe random and sudden onsets of photochemical reactions which substantially altered all parts of the wing (*b–d*). The reactions were accompanied by a strongly increased, flickering luminescence. We note that photochemical processes may take place to an appreciably different extent and at varying power conditions, depending on the sample.

## 4. Conclusion

Multifocal multiphoton microscopy is an interesting alternative to standard confocal and multiphoton scanning microscopy. As the foci in MMM do not cross-talk, MMM features the same spatial resolution as its standard two-photon and confocal single-beam counterparts. The examples shown in this paper demonstrate that, with the exception of strongly scattering samples, large stacks of sharp images can be recorded within seconds, as opposed to minutes in other systems. We also note that the system can still be technically improved in terms of speed and sensitivity for example by appropriate antireflection coating of the optical components. Importantly, MMM allows direct viewing of the plane of interest in the interior of the specimen. Thus, it allows for a very intuitive way of interacting with the specimen. Apart from the necessity of

using a pulsed mode laser, MMM offers a most simple and straightforward means of producing 3-D images. Its key features are efficient use of light, real-time imaging and direct view. These make it highly attractive for biological microscopy in the immediate future.

## Acknowledgments

We would like to thank P Lodemann, P Holroyd and Dr W Zuschratter for the preparation of samples and for useful discussions. We are grateful to M Nagorni and M Glatz for technical assistance and also acknowledge useful discussions with A Egner and A Schönle. D Stalling (Konrad-Zuse-Zentrum für Informationstechnik Berlin) kindly provided us with the *Amira* 3-D visualization and modelling program. We also thank Olympus (Hamburg) for lending us their water immersion lens.

## References

[1] Pawley J 1995 *Handbook of Biological Confocal Microscopy* (New York: Plenum)
[2] Denk W, Piston D W and Webb W W 1995 *Two-Photon Molecular Excitation in Laser Scanning Microscopy* ed J Pawley (New York: Plenum) pp 445–58
[3] Denk W, Strickler J H and Webb W W 1990 Two-photon laser scanning fluorescence microscopy *Science* **248** 73–6
[4] Hell S and Stelzer E H K 1992 Fundamental improvement of resolution with a 4Pi-confocal fluorescence microscope using two-photon excitation *Opt. Commun.* **93** 277–82
[5] Hell S W, Bahlmann K, Schrader M, Soini A, Malak H, Gryczynski I and Lakowicz J R 1996 Three-photon excitation in fluorescence microscopy *J. Biomed. Opt.* **1** 71–3
[6] Stelzer E H K, Hell S, Lindek S, Pick R, Storz C, Stricker R, Ritter G and Salmon N 1994 Non-linear absorption extends confocal fluorescence microscopy into the ultra-violet regime and confines the illumination volume *Opt. Commun.* **104** 223–28
[7] Wokosin D L, Centonze V E, Crittenden S and White J 1996 Three-photon excitation fluorescence imaging of biological specimens using an all-solid-state laser *Bioimaging* **4** 208–14
[8] Xu C, Zipfel W, Shear J B, Williams R M and Webb W W 1996 Multiphoton fluorescence excitation: new spectral windows for biological nonlinear microscopy *P.N.A.S. USA* **93** 10763–8
[9] Curley P F, Ferguson A I, White J G and Amos W B 1992 Applications of a femtosecond self-sustained mode-locked Ti:sapphire laser to the field of laser scanning confocal microscopy *Opt. Quantum Electron.* **24** 851–9
[10] Niemz M 1996 *Laser-Tissue Interaction* (Berlin: Springer)
[11] König K, Hong L, Berns M W and Tromberg B J 1995 Cell damage by near-IR microbeams *Nature* **377** 20–21
[12] Bewersdorf J and Hell S W 1997 Picosecond pulsed two-photon imaging with repetition rates of 200 and 400 MHz *J. Microsc.* **191** 28–38
[13] Hell S W, Booth M, Wilms S, Schnetter J C M, Kirsch A K, Arndt-Jovin D J and Jovin T 1998 Two-photon near and far-field fluorescence microscopy with continuous-wave excitation *Opt. Lett.* **23** 1238–40
[14] Hell S W 1998 Rastermikroskop bei dem eine Probe mit mehreren Punkten gleichzeitig angeregt wird *German Patent Application* DE 196 53 413 (filed 1996, published 1998)
[15] Bewersdorf J, Pick R and Hell S W 1998 Multifocal multiphoton microscopy *Opt. Lett.* **23** 655–7
[16] Straub M and Hell S W 1998 Fluorescence lifetime three-dimensional microscopy with picosecond precision using a multifocal multiphoton microscope *Appl. Phys. Lett.* **73** 1769–71
[17] Buist A H, Müller M and Brakenhoff G J 1998 Real-time two-photon microscopy *SPIE Photonics West* (oral presentation)
[18] Brakenhoff G J, Squier J, Norris T, Bliton A C, Wade M H and Athey B 1996 Real-time two-photon confocal microscopy using a femtosecond, amplified Ti:sapphire system *J. Microsc.* **181** 253–9
[19] Andersen P and Trommald M 1995 Possible strategies for finding the substrate for learning induced chnages in the hippocampal cortex *J. Neurobiol.* **26** 396–402
[20] Kolb B and Wishaw I Q 1998 Brain plasticity and behavior *Ann. Rev. Psych.* **49** 43–64
[21] Bevilaqua F, Marquet P, Depeursinge C and Haller E B 1995 Determination of reduced scattering and absorption coefficients by a single charge-coupled device array measurement, part II: measurements on biological tissues *Opt. Eng.* **34** 2064–9
[22] Okada E, Schweiger M, Arridge S R, Firbank M and Delpy D T 1996 Experimental validation of Monte Carlo and finite-element methods for the estimation of the optical path length in inhomogenous tissue *Appl. Opt.* **35** 3362–71
[23] König K, So P T C, Mantulin W W, Tromberg B J and Gratton E 1996 Two-photon excited lifetime imaging of autofluorescence in cells during UVA and NIR photostress *J. Microsc.* **183** 197–204

## Appendix A

Parameters used for preparation and observation in each experiment are listed in the table overleaf.

**Table A1.**

| Fig. | Sample | Stains | Wave-length (nm) | Number of foci | Average power per focus (mW) | Objective [type, NA] | Tube lens | Filter combination | Number of slices | Distance between slices (nm) | Exposure time per slice (ms) |
|---|---|---|---|---|---|---|---|---|---|---|---|
| 2 | *Prionium* | safranin-fast green | 895 | 15 | 7.0 | Leica PL APO oil immersion (100×, NA 1.4) | 1.0× | 2 interference filters plus 1 mm KG3 and 3 mm OG590/ 2 mm BG 39 | 41 | 790 | 200 |
| 3 | PC12 | acridine orange | 895 | 15 | 7.0 | Olympus Uplan APO water immersion (60×), NA 1.2) | 1.6× | 2 interference filters plus 1 mm KG3 and 3 mm OG590 or a D520/60 interference filter | 31 | 1040 | 75 or 200 |
| 4 | gerbil neuronal cells | Lucifer Yellow antibodies plus FITC | 780 | 20 | 5.5 | Olympus Uplan APO water immersion (60×), NA 1.2) | 1.6× | 2.5 mm BG 39 | 61 | 410 | 1000 |
| 5 | wing of *Drosophila melanogaster* | | 775 | 25 | 1.8/3.8 | Leica PL FLUOTAR oil immersion (40×), NA 1.0) | 1.6× | 3 mm BG 39 | 168 | 0 | 2000 |